THE ASTRONOMICAL JOURNAL, 118:145–161, 1999 July

MOLECULAR GAS IN STRONGLY INTERACTING GALAXIES. I. CO (1–0) OBSERVATIONS

MING ZHU,[1] E. R. SEAQUIST,[1] EMMANUEL DAVOUST,[2] DAVID T. FRAYER,[3] AND HOWARD A. BUSHOUSE[4]

Received 1999 March 17; accepted 1999 March 30

ABSTRACT

We present observations of the CO (1–0) line in 80 interacting galaxies as part of a program to study the role of interactions and mergers in triggering starbursts. The sample, which only includes obviously interacting pairs of galaxies, is the largest such sample observed in CO. The observations were carried out at the NRAO 12 m and IRAM 30 m telescopes. CO emission was detected in 56 galaxies (of which 32 are new detections), corresponding to a detection rate of 70%. Because most galaxies are slightly larger than the telescope beam, correction factors were applied to include CO emission outside the beam. The correction factors were derived by fitting a Gaussian function or an exponential CO brightness distribution to galaxies with multiple pointings and by assuming an exponential model for galaxies with single pointing. We compared the global CO fluxes of 10 galaxies observed by us at both telescopes. We also compared the measured fluxes for another 10 galaxies observed by us with those by other authors using the NRAO 12 m and FCRAO 14 m telescopes. These comparisons provide an estimate of the accuracy of our derived global fluxes, which is ~40%. Mapping observations of two close pairs of galaxies, UGC 594 (NGC 317) and UGC 11175 (NGC 6621), are also presented. In subsequent papers we will report the statistical analyses of the molecular properties in our sample galaxies and make comparisons between isolated spirals and interacting galaxies.

Key words: galaxies: interactions — ISM: molecules

1. INTRODUCTION

Galaxy interactions and mergers are thought to play a key role in triggering starbursts. Sanders et al. (1988) found that all galaxies with *IRAS*-derived far-infrared luminosities larger than $10^{12}\ L_{\odot}$ are interacting galaxies or mergers. CO observations of the IR-luminous mergers (Solomon & Sage 1988; Sanders, Scoville, & Soifer 1991) show that most of them are very rich in molecular gas. Obviously, the merging of two gas-rich galaxies can trigger intense starburst activity and produce extremely high luminosity infrared radiation. This process has been successfully modeled by numerical simulations (Barnes & Hernquist 1991; Mihos & Hernquist 1994). An important question is whether the large amounts of molecular gas in *IRAS*-luminous mergers are the result of galaxy interactions. In other words, can galaxy interaction somehow act to build up more molecular gas to fuel a starburst?

Many CO studies of external galaxies have reported that the M_{H_2}/L_B ratio is enhanced in interacting galaxies (IGs) compared with isolated galaxies (Solomon & Sage 1988; Young et al. 1996; Braine & Combes 1993; Combes et al. 1994). However, all the previous studies were based on a relatively small sample, and the IGs were often selected according to their *IRAS* fluxes, which produces a bias toward gas-rich galaxies. A statistically meaningful conclusion requires a well-defined optically selected sample of interacting systems that is sufficiently large to cover different galaxy progenitor types, interaction phases, and encounter geometries.

We have started a systematic study of the molecular gas properties in IGs, which includes two parts: (1) a CO (1–0) survey of a large optically selected sample in order to make clear whether the CO emission is enhanced in IGs and whether this is associated with all IG types; (2) an analysis of the excitation conditions in selected galaxies with multi-transition CO data to investigate whether the enhanced CO emission in some systems is a result of higher excitation. Our studies are also aimed at answering the question of whether the enhanced star formation activity in IGs is due to a higher abundance of molecular gas or to a higher star formation efficiency.

We have completed a CO (1–0) survey of 80 interacting galaxies with the NRAO 12 m and IRAM 30 m telescopes. CO (2–1) and CO (3–2) data have also been obtained with the James Clerk Maxwell Telescope and the NRAO 12 m telescope for a subsample of interacting systems. In addition, we have mapped the CO (1–0) distribution in several galaxies using the Owens Valley Radio Observatory (OVRO) interferometer and the IRAM 30 m telescope. In this paper we present the data from our CO (1–0) survey. The statistical analyses and detailed studies of the molecular gas properties will be reported in subsequent papers.

2. THE SAMPLE

The majority of our sample galaxies are from the sample by Bushouse (1986). This sample includes only pairs of galaxies that exhibit features unmistakably associated with strong tidal interactions (e.g., tidal tails, bridges, and warped disks). Thus the selection is based on morphology alone, and not on a priori knowledge of levels of IR or radio emission. Therefore, the sample should not be biased toward gas-rich or starburst galaxies.

We chose all the galaxies in Bushouse's sample with $B_T < 14.5$, except those with $L_B < 1 \times 10^9\ L_{\odot}$. The gas in dwarf galaxies may not be gravitationally bound and may have a different response to tidal interactions. Thus we will study them separately. We extended the Bushouse sample

[1] Department of Astronomy, University of Toronto, 60 Saint George Street, Toronto, ON M5S 3H8, Canada.
[2] Observatoire Midi-Pyrénées, 14 Avenue Edouard Belin, F-31400 Toulouse, France.
[3] Department of Astronomy, California Institute of Technology, 105-24, Pasadena, CA 91125.
[4] Space Telescope Science Institute, 3700 San Martin Drive, Baltimore, MD 21218.

TABLE 1

SOURCE INFORMATION

Name	Other Name	R.A. (1950)	Decl. (1950)	cz (km s^{-1})	W_{25} [a] (km s^{-1})	D [b] (Mpc)	B_T^0	D_{25} (arcmin)	r_b (arcmin)	Type
UGC 365	NGC 169	00 34 13.7	+23 43 00.0	4627	611	63.6	12.40	2.6	0.7	SA(s)ab?sp
UGC 480 W		00 43 48.5	+36 03 11.6	11173	547	151.2	12.97	1.5	1.2	S?
UGC 480 E		00 43 55.3	+36 03 31.0	11093	547	150.2	14.81	0.8	0.4	S?
UGC 593	NGC 317A	00 54 49.8	+43 31 50.8	5293	416	72.9	14.60	1.4	1.3	S?
UGC 594	NGC 317B	00 54 51.3	+43 31 18.8	5334	416	73.4	12.80	1.1	0.5	SB?
UGC 717		01 06 44.4	+14 04 14.5	11034	228	148.6	13.94	1.5	0.9	SBb
UGC 813		01 13 20.0	+46 28 35.0	4994	637	68.8	13.67	1.2	0.5	S?
UGC 816		01 13 24.3	+46 29 01.0	5188	637	71.5	13.16	1.9	0.9	S?
UGC 979	NGC 523	01 22 29.8	+33 45 53.0	4750	...	65.5	12.60	2.5	0.7	Pec
UGC 1063...........	NGC 569	01 26 28.7	+10 52 22.0	5772	336	78.2	13.75	1.0	0.5	S?
UGC 1430...........	NGC 750/1	01 54 37.6	+32 58 00.0	5222	...	71.3	12.65	1.7	1.3	E pec
UGC 1810...........		02 18 23.7	+39 08 50.0	7563	...	102.4	12.91	2.2	1.5	SA(s)b pec
UGC 3031...........	NGC 1568A	04 21 45.0	−00 51 00.0	4734	554	62.3	14.60	1.6	0.5	S?
UGC 3032...........	NGC 1568	04 21 51.0	−00 52 00.0	4734	246	62.3	14.15	1.1	0.8	S0+ pec?
UGC 3706 N........		07 06 09.0	+47 59 41.0	6090	348	81.2	14.10	0.4	0.2	Sa
UGC 3706 S		07 06 10.3	+47 59 21.0	6090	348	81.2	14.10	0.4	0.2	Sa
UGC 4264...........	NGC 2535	08 08 13.1	+25 21 23.0	4099	178	53.8	12.64	2.5	1.2	SA(r)c pec
UGC 4653...........		08 50 46.3	+35 20 18.2	16560	...	220.4	14.02	1.9	1.1	SB(s)b
UGC 4718...........	NGC 2719	08 57 07.4	+35 55 34.0	3157	...	41.8	13.60	1.4	0.3	Im pec
UGC 4744 W	NGC 2735	08 59 41.9	+26 07 56.2	2450	416	31.8	13.38	1.2	0.4	SAB(rs)b pec
UGC 4744 E	NGC 2735A	08 59 45.2	+26 08 10.0	2830	421	37.7	0.00	0.2	0.2	Im? pec
UGC 4757...........	NGC 2744	09 01 49.7	+18 39 52.2	3428	267	44.4	13.55	1.7	1.1	SB(s)ab*P
UGC 5265...........	NGC 3018	09 47 07.1	+00 51 22.0	1863	171	22.8	13.61	1.2	0.7	SB(s)b pec?
UGC 5269...........	NGC 3023	09 47 18.2	+00 51 12.0	1879	149	23.0	12.90	2.9	1.5	SAB(s)c pec?
UGC 53045		09 50 30.1	+08 06 08.9	12306	...	164.1	13.98	0.9	0.8	S?
UGC 5600...........		10 19 16.5	+78 52 54.9	2823	177	39.5	14.14	1.4	1.0	S0?
UGC 5609...........		10 19 31.9	+78 51 48.0	2729	177	38.2	14.15	1.3	0.8	S?
UGC 5773...........		10 34 17.9	+18 32 48.0	6160	258	82.1	14.00	0.6	0.4	S?
UGC 5931...........	NGC 3395	10 47 02.7	+33 14 44.0	1620	216	21.3	12.09	2.1	1.2	SAB(rs)cd pec:
UGC 5935...........	NGC 3396	10 47 08.9	+33 15 18.0	1625	...	21.5	12.32	3.1	1.2	IBm pec
UGC 5984...........		10 49 29.6	+30 19 26.0	10423	399	138.6	14.10	1.9	1.2	S?
UGC 6134...........	NGC 3509	11 01 48.5	+05 06 01.0	7704	469	101.1	12.78	2.1	0.9	SA(s)bc: pec
UGC 6527...........		11 29 55.4	+53 13 35.0	8208	478	109.1	15.32	1.1	0.3	Sa pec
UGC 6643...........	NGC 3808	11 38 07.9	+22 42 18.0	7078	293	93.8	13.66	1.7	0.9	SAB(rs)c: pec
UGC 7085A S		12 03 12.5	+31 20 14.0	7005	139	93.3	15.00	2.6	1.0	SA0$^-$ pec
UGC 7085A N......		12 03 12.6	+31 21 27.0	6949	214	92.6	0.00	0.4	0.3	SAB0$^-$ pec?
UGC 7230 N........		12 11 07.0	+16 24 10.0	7128	225	94.4	14.05	1.4	0.9	SB(s)d pec
UGC 7230 S		12 11 05.1	+16 23 49.0	7128	225	94.4	14.05	1.4	0.9	SB(s)d pec
UGC 7277 S	NGC 4211	12 13 05.8	+28 26 51.0	6670	124	88.8	15.20	1.5	1.5	S0/a pec
UGC 7277 N........	NGC 4211	12 13 04.4	+28 27 20.0	6599	574	87.9	14.30	1.0	1.0	S0/a pec
UGC 7905 S		12 41 31.9	+55 10 11.2	4933	209	67.0	13.97	1.0	0.6	Pec
UGC 7905 N........		12 41 33.4	+55 10 44.4	4875	324	66.2	13.97	0.0	1.0	S? pec
UGC 8357 S		13 15 25.1	−00 02 56.0	9944	...	132.6	13.84	1.2	0.5	SB(s)b pec?
UGC 8528...........	NGC 5216	13 30 23.6	+62 57 25.7	2949	...	41.0	13.49	2.5	1.5	E0 pec
UGC 8529...........	NGC 5218	13 30 27.8	+63 01 27.0	2807	...	39.1	12.85	1.8	1.3	SB(s)b? pec;LNR
UGC 8677...........	NGC 5278	13 39 47.9	+55 55 18.0	7541	...	102.6	13.40	1.4	0.9	SA(s)b? pec
UGC 8774 N........	NGC 5331	13 49 43.7	+02 21 17.0	9906	527	131.6	13.83	1.1	0.7	Sb pec?
UGC 8774 S	NGC 5331	13 49 43.6	+02 20 53.0	9906	527	131.6	14.85	1.1	0.7	Sb pec?
UGC 8849 S		13 53 35.4	+17 44 36.0	6442	...	85.9	14.50	0.9	0.0	disrupted spiral
UGC 8849 N........		13 53 36.5	+17 45 21.0	6103	...	81.4	14.50	0.7	0.2	S0
UGC 8898...........	NGC 5394	13 56 25.1	+37 41 45.7	3427	...	46.7	13.29	1.7	1.0	SB(s)b pec
UGC 8900...........	NGC 5395	13 56 29.8	+37 40 05.0	3487	626	47.5	12.01	2.9	1.5	SA(s)b pec
UGC 8929 S		13 58 48.5	+21 28 44.0	8353	...	111.4	14.70	0.6	0.4	S?
UGC 8931...........	NGC 5410	13 58 49.8	+41 13 45.0	3738	278	51.0	13.53	1.5	0.8	SB?
UGC 8941 N........	NGC 5421	13 59 30.0	+34 04 10.0	7889	282	106.1	14.10	1.2	0.9	SB?
UGC 8941 S	NGC 5421	13 59 30.9	+34 03 45.0	7868	282	106.1	15.00	1.2	0.9	E
UGC 9001...........		14 02 26.6	+11 02 27.0	11234	...	149.8	14.40	1.0	0.4	SB?
UGC 9000...........		14 02 24.2	+11 02 51.0	5516	584	149.8	14.21	1.0	0.2	SB?
UGC 9102...........	NGC 5514	14 11 10.6	+07 53 32.0	7300	259	97.4	13.19	2.2	1.1	SA
UGC 9142...........	NGC 5544	14 14 57.5	+36 48 11.0	3077	273	42.2	13.20	1.0	0.9	(R)SB(rs)0
UGC 9226...........	NGC 5614	14 22 01.1	+35 05 04.0	3892	161	53.0	12.37	2.5	2.0	SA(r)ab pec
UGC 9507...........	NGC 5755	14 43 26.2	+38 59 23.0	9604	...	129.4	14.50	1.3	1.0	SB?
UGC 9525...........		14 44 51.7	+13 39 56.0	8400	...	112.0	14.40	1.5	0.7	S?

TABLE 1—*Continued*

Name	Other Name	R.A. (1950)	Decl. (1950)	cz (km s^{-1})	W_{25}[a] (km s^{-1})	D[b] (Mpc)	B_T^0	D_{25} (arcmin)	r_b (arcmin)	Type
UGC 9851	NGC 5930	15 24 18.9	+41 50 53.0	2672	...	37.4	12.56	1.7	0.9	SAB(rs)b pec
UGC 9903	NGC 5953	15 32 13.2	+15 21 40.0	1965	261	27.2	13.00	1.6	1.4	SAa?; Pec
UGC 9904	NGC 5954	15 32 15.9	+15 22 00.0	1959	257	27.1	13.10	1.3	0.6	SAB(rs)cd? pec
UGC 10033	NGC 5996	15 44 43.2	+18 02 15.0	3304	200	45.2	12.67	1.7	0.9	S?
UGC 10267	NGC 6090	16 10 24.3	+52 35 04.0	8785	396	119.4	13.39	1.7	0.7	Sd pec; H II
UGC 10610		16 53 24.9	+43 08 22.0	9934	193	134.8	14.53	2.2	0.9	SB?
UGC 10607	IC 4630	16 53 08.0	+26 44 30.0	10359	...	140.1	13.96	1.1	0.8	S?
UGC 10675		17 01 21.6	+31 31 39.0	10000	167	135.5	14.89	0.7	0.4	S?
UGC 10923		17 36 22.7	+86 46 39.0	7721	541	105.3	13.70	1.2	0.7	S?
UGC 11137	NGC 6570	18 08 50.4	+14 04 52.0	2287	226	32.5	12.31	1.8	1.1	SB(rs)m?
UGC 11175 S	NGC 6622	18 13 14.4	+68 20 15.0	6284	404	86.2	...	0.5	0.4	Sa
UGC 11175 N......	NGC 6621	18 13 14.4	+68 20 55.0	6284	482	86.2	13.40	2.1	0.8	Sb pec
UGC 11391	NGC 6745	19 00 03.2	+40 40 23.4	4545	446	63.5	13.90	1.5	0.7	S?
UGC 11414	NGC 6786	19 11 53.2	+73 19 30.0	7510	...	103.2	13.19	1.1	0.9	SB?
UGC 11657		20 57 11.7	−02 04 57.0	5836	224	79.8	14.10	1.1	1.1	Pec
UGC 11658		20 57 12.8	−02 04 07.0	5843	...	79.9	13.90	1.4	0.9	SAB(rs)a pec?
UGC 11695		21 09 35.4	−01 40 51.0	9672	510	130.9	14.07	1.4	0.8	SA(rs)b pec?
UGC 11984	NGC 7253	22 17 08.5	+29 08 50.0	4583	...	64.0	13.30	1.7	0.5	SB?
UGC 11985	NGC 7253	22 17 13.6	+29 08 20.0	4493	...	62.7	13.30	1.6	0.5	S?
UGC 12066		22 29 26.4	+19 26 05.0	5587	594	77.1	13.82	1.1	0.7	S
UGC 12456	NGC 7550	23 12 46.8	+18 41 19.2	5101	...	70.4	13.11	1.4	1.2	SA0-
UGC 12457	NGC 7549	23 12 48.0	+18 46 07.6	4686	317	64.8	12.67	2.8	0.7	SB(s)cd pec
UGC 12908	NGC 7805	23 58 53.1	+31 09 20.0	4850	...	67.1	13.90	1.2	0.9	SAB0^0: pec
UGC 12911	NGC 7806	23 58 56.4	+31 09 51.0	4768	349	66.0	13.88	1.1	0.8	SA(rs)bc? pec
UGC 12914		23 59 04.4	+23 12 22.0	4371	628	60.6	12.51	2.3	1.3	(R)S(r)cd? pec
UGC 12915		23 59 08.4	+23 13 00.0	4336	571	60.2	13.01	1.5	0.5	S?

[a] W_{25} is the full width of the emission line at 25% of the mean flux level. The data are mostly from Bushouse 1987 when available. The others are from the RC3 or NED.
[b] The distance was calculated using the galactocentric velocity from the RC3 and assuming $H_0 = 75$ km s^{-1} Mpc^{-1}.

by choosing interacting systems from the UGC catalog (Nilson 1973) with the same selection criteria. The final sample selected for our CO (1–0) observations depended on the source availability during the observing runs.

As discussed by Bushouse (1986), these selection criteria are possibly biased toward late-stage IGs, because N-body simulations show that the timescale for developing tidal tails and bridges is around 10^8 yr (Toomre & Toomre 1972; Barnes & Hernquist 1992). Also, the presence of long tails indicates that the mass ratios of many of the galaxy pairs are near unity. Finally, the majority of the IGs in this sample do not reside in regions of high galactic density, as serious morphological disturbances of the kind selected require slow, parabolic passages of the galaxies (Tremaine 1981). These are conditions not usually found in groups or clusters of galaxies, where the relative velocities are high.

Table 1 lists the basic parameters for all 80 of the observed galaxies, including the name, central position, distance, heliocentric H I velocity (or optical velocity if H I data were not available), and 25% line width from the RC3 catalog (de Vaucouleurs et al. 1991), corrected total blue magnitude B_T^0 from RC3, D_{25}, and r_b, which are the sizes along the major and minor axes. The last column is the Hubble type from RC3.

CO (1–0) data are available in the literature for ∼40 other interacting systems. In Paper II we will combine these data with our own in Table 1 to investigate the molecular gas content with a final sample containing 120 galaxies. This is the largest available CO sample of strongly interacting galaxies in the northern sky with declination greater than $-10°$ and $B_T < 14.5$.

3. CO OBSERVATIONS

3.1. *Observations with the NRAO* 12 m *Telescope*

We observed the strong and extended sources in the CO (1–0) transition with the NRAO 12 m telescope[5] at Kitt Peak (Arizona) during the observing runs in 1997 July and 1998 February under generally good weather conditions. The single-sideband system temperatures ranged from 260 to 500 K depending primarily on the weather. We used the dual-channel mode with two 3 mm SIS receivers to observe the CO (1–0) line in both left and right circular polarizations. Each receiver was connected to a 256 × 2 MHz filter bank, which gives a spectral resolution of 5.2 km s^{-1} and a velocity coverage of 1336 km s^{-1} at the frequency of CO (1–0) line. Cold-load calibrations were made after every 5 minutes of integration. The focus of the telescope was checked two or three times a day and the pointing was checked every 1–2 hr using bright quasars and planets. The rms pointing error was 8″, which may be compared with the telescope beamwidth of 55″ (FWHM) at 115 GHz. Beam switching with a beam throw of 4′ in azimuth at a frequency of 1.25 Hz was used for all observations, which yields very flat baselines in most spectra. As a result, only linear baselines had to be removed from our data.

For most galaxies with an angular size less that 2′, the 55″ telescope beam size covered most of the CO emission, and

[5] The National Radio Astronomy Observatory is a facility of the National Science Foundation, operated under cooperative agreement by Associated Universities, Inc.

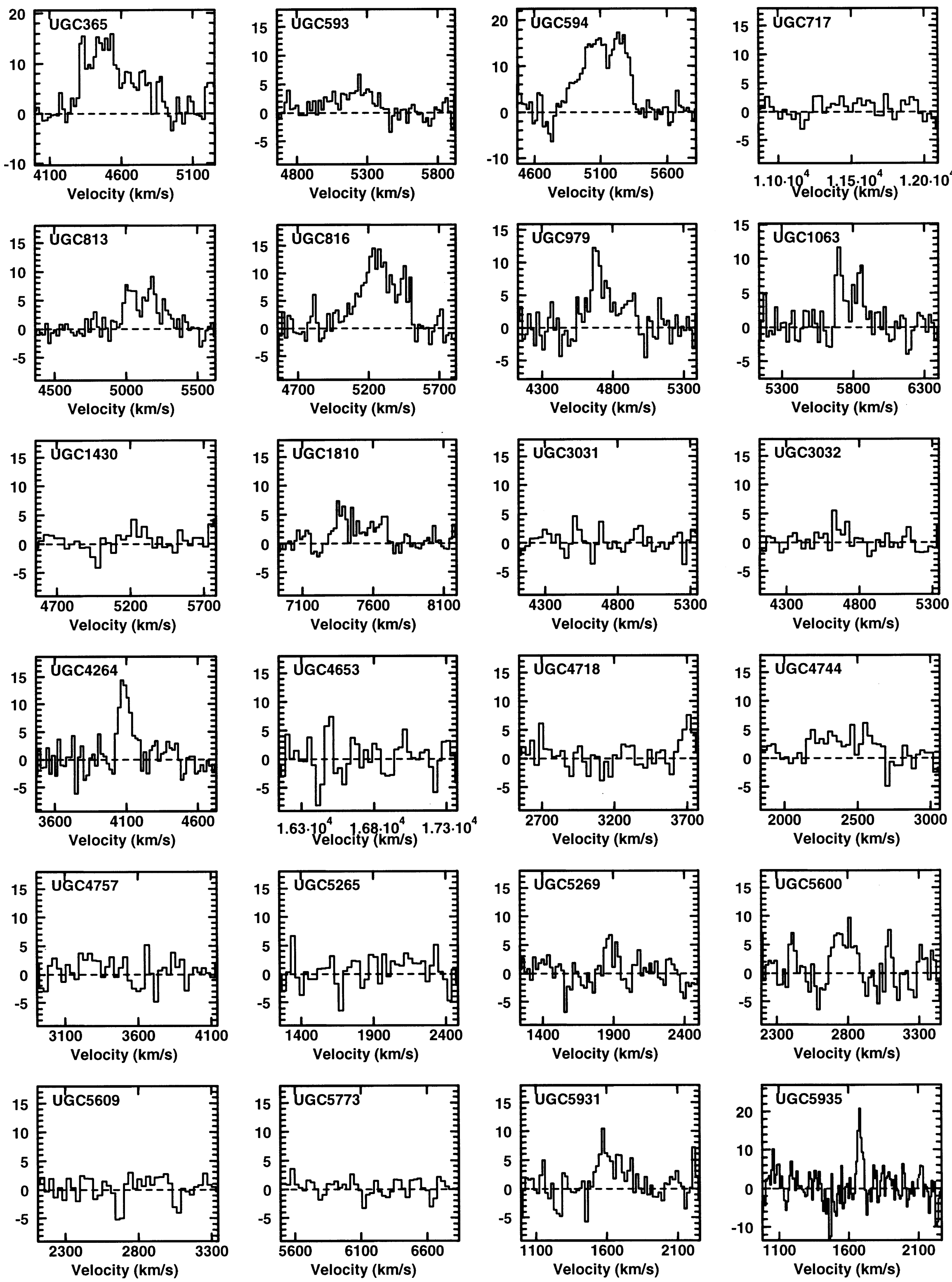

FIG. 1.—CO (1–0) Spectra of interacting galaxies observed with the NRAO 12 m telescope. The vertical scale is main-beam brightness temperature $T_{\rm mb}$ in mK. The velocity is heliocentric optical velocity.

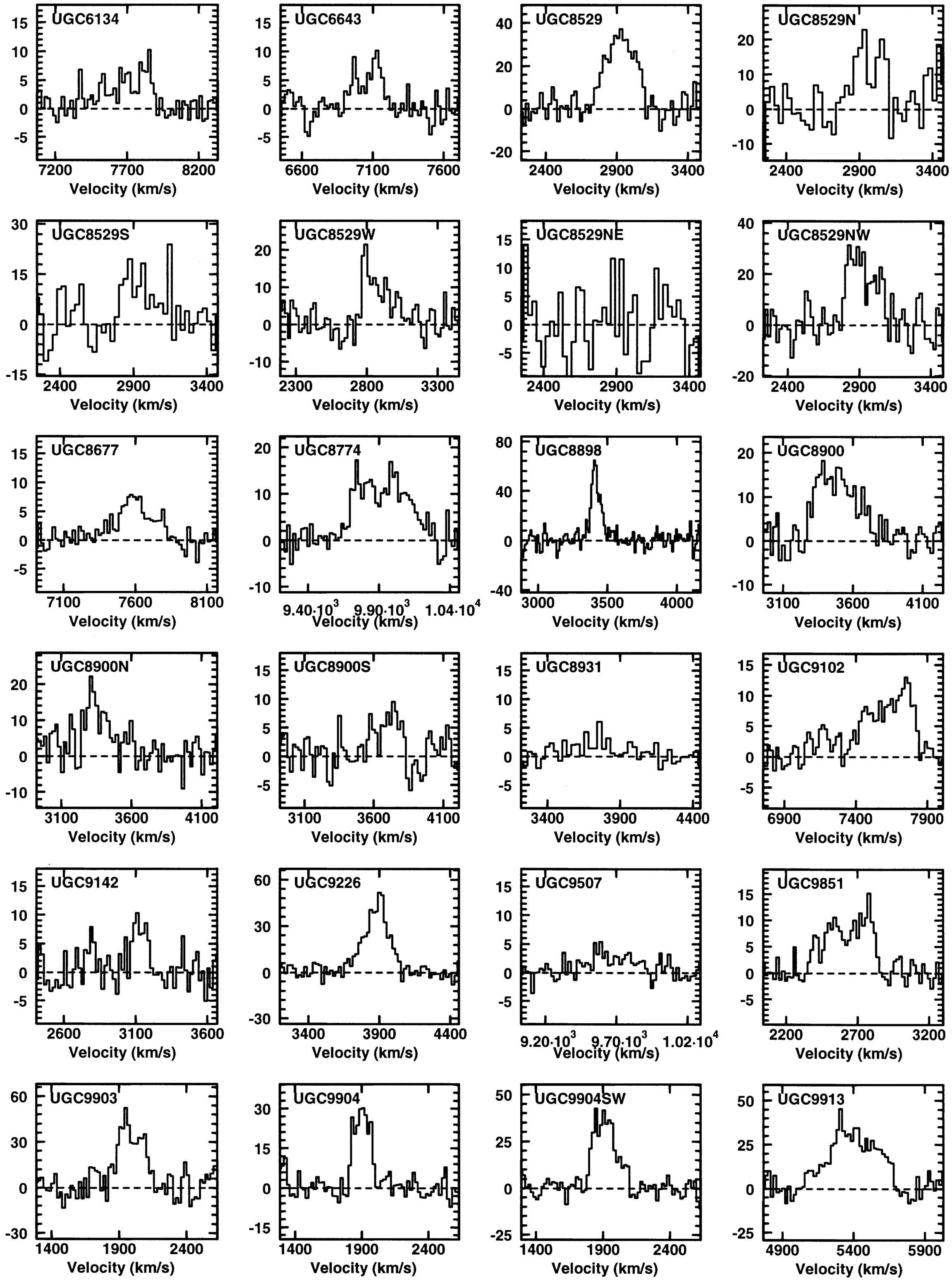

FIG. 1.—*Continued*

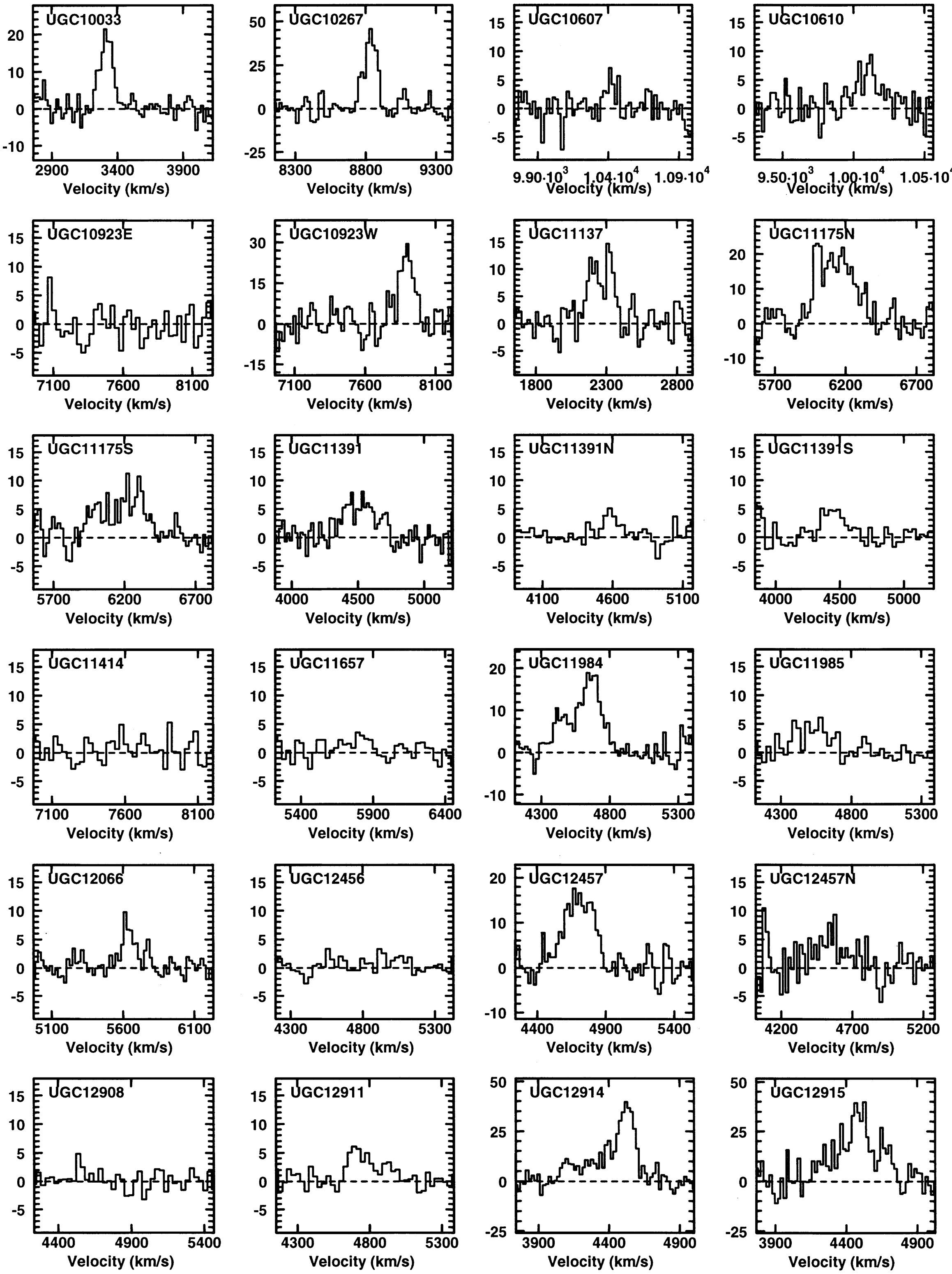

FIG. 1.—*Continued*

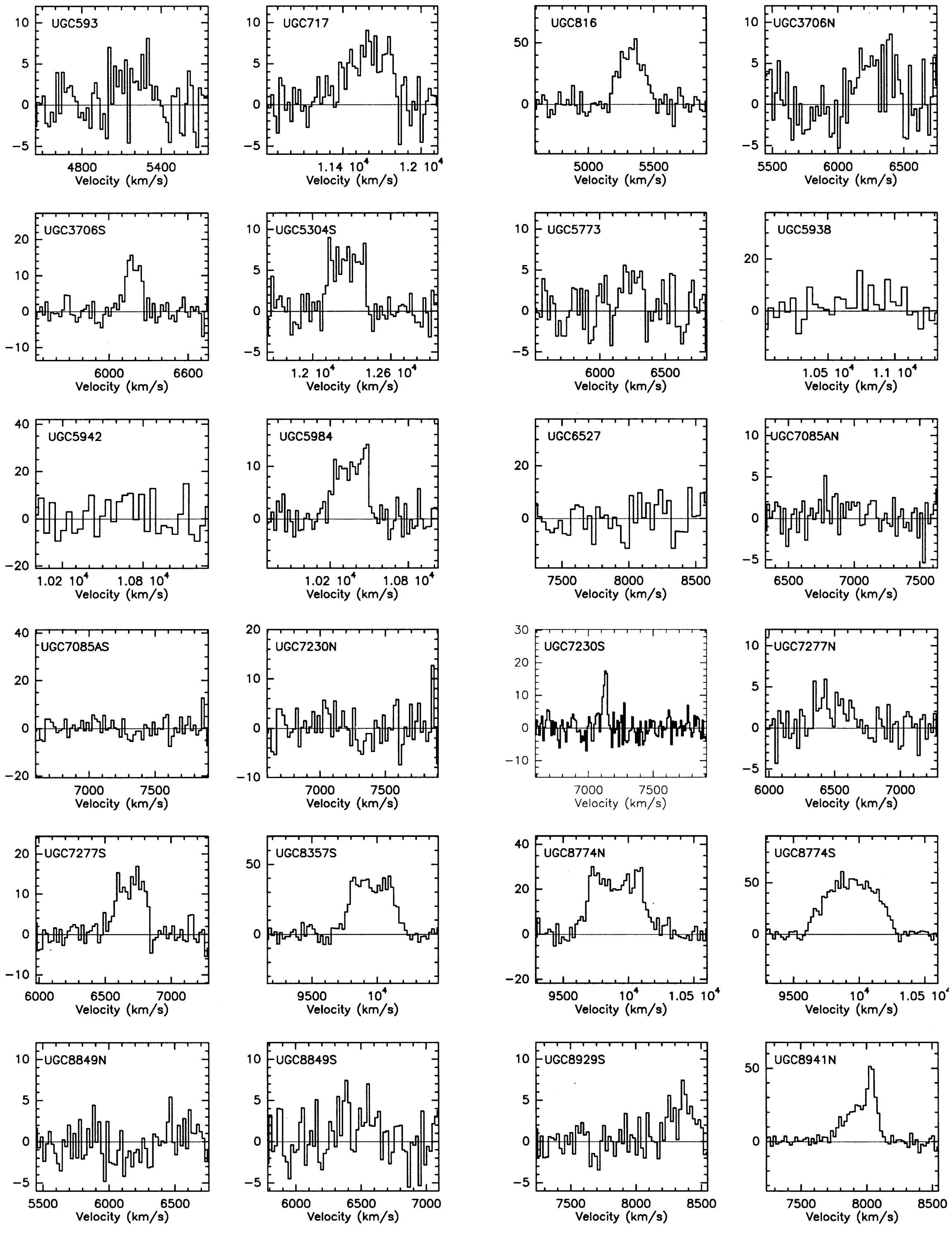

FIG. 2.—(1–0) Spectra of interacting galaxies observed with the IRAM 30 m telescope. The vertical scale is main-beam brightness temperature T_{mb} in mK. The velocity is the heliocentric optical velocity.

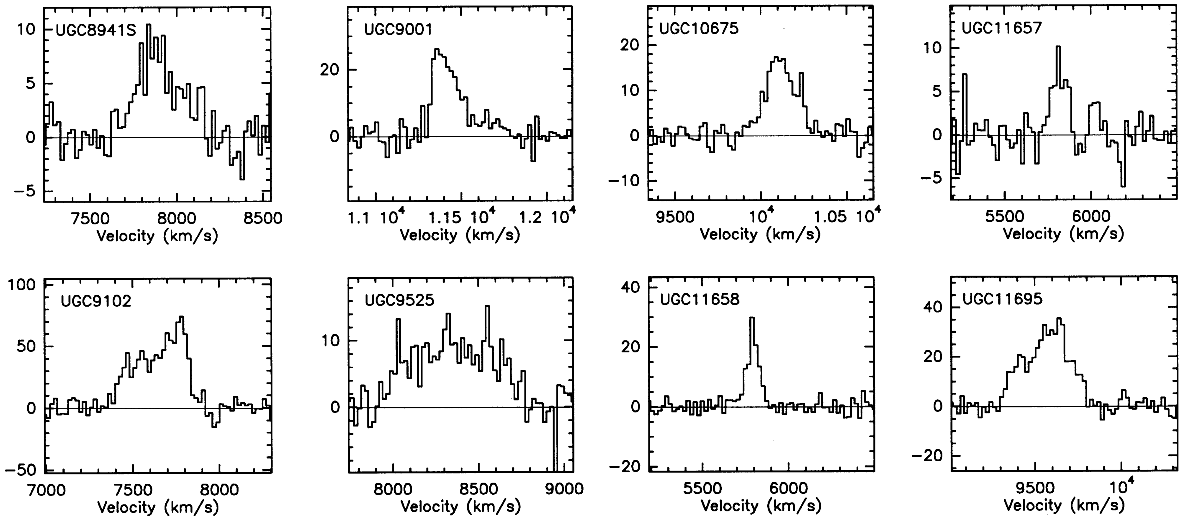

FIG. 2.—*Continued*

consequently, we observed them only at single positions. The sources larger than 2′ were sampled at several points along the major axis. We integrated typically for 1–2 hr at each point. Figure 1 shows the final spectra reduced with the NRAO software UNIPOPS. The spectra were smoothed to a resolution of 20 km s^{-1}, except for several galaxies with a narrow spectral line, which were smoothed to a resolution of 10 km s^{-1}. We converted the temperature scale from T_R^* to $T_{\rm mb}$ (main-beam temperature) using the formula $T_{\rm mb} = T_R^*/\eta_m$, where the main beam efficiency $\eta_m = 0.88$ was taken from the user's manual for the 12 m telescope.

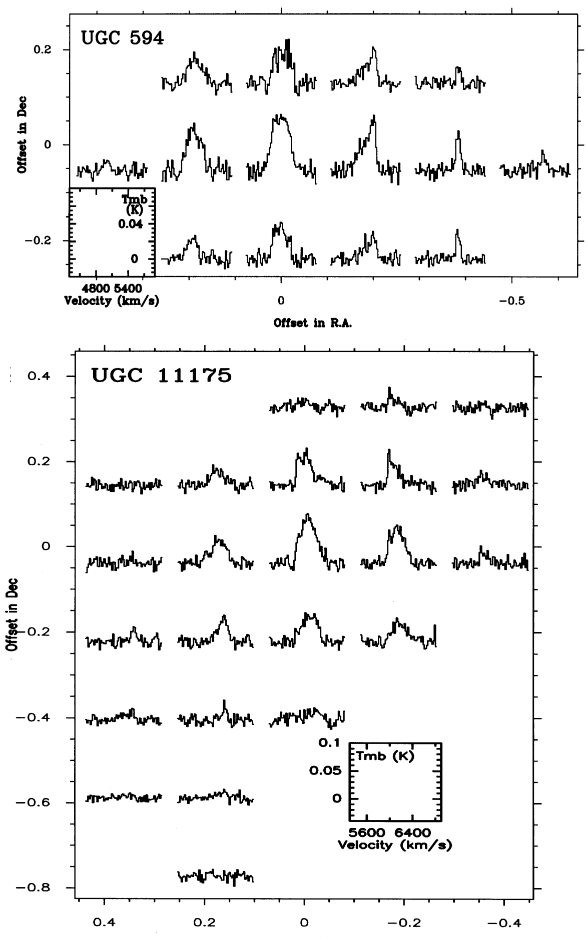

FIG. 3.—CO (1–0) grid spectra of UGC 594 (*top*) and UGC 11175 (*bottom*) observed with the IRAM 30 m telescope with 11″ sampling. The offsets are in arcminutes.

3.2. *Observations with the IRAM* 30 m *Telescope*

A total of 26 galaxies were observed with the IRAM 30 m telescope[6] at Pico Veleta (Spain) in 1998 June. This sample comprised primarily more distant and therefore fainter galaxies than those observed with the NRAO 12 m. CO (1–0) and CO (2–1) lines were observed simultaneously with two 3 mm SIS receivers and one 1 mm receiver. The 1 mm receiver and one of the 3 mm receivers are the new-generation receivers A230 and A100. The weather was excellent and stable during the observing run, and thus we performed cold-load calibrations every 15 minutes. The new receivers are very stable and had system temperatures of typically 200–300 K at 3 mm (115 GHz) and 250–500 K at 1 mm (230 GHz). We used two 512 x 1 MHz filter bank spectrometers for the 3 mm receivers and the autocorrelator for A230. Here we discuss only the CO (1–0) observations. The CO (2–1) data will be reported in a separate paper. The spectral resolution is 2.6 km s^{-1}, and velocity coverage is 1336 km s^{-1} at the frequency of CO (1–0) line.

The focus was checked every day after sunrise and sunset, and the pointing accuracy was checked every 1–2 hr using bright quasars and planets. The rms pointing error was $\sim 3''$, which may be compared with the telescope beam-width of 22″ at 115 GHz. Beam switching with a beam throw of 70″ in azimuth at a frequency of 0.25 Hz was used for all observations, which yielded a very flat baseline in most spectra. As a result, only linear baselines were removed for most cases, except for some spectra from the 3 mm 2 receiver, for which a second-order polynomial baseline was removed.

[6] The 30 m telescope at Pico Veleta, Spain, is operated by Institut de Radio Astronomie Millimétrique (IRAM).

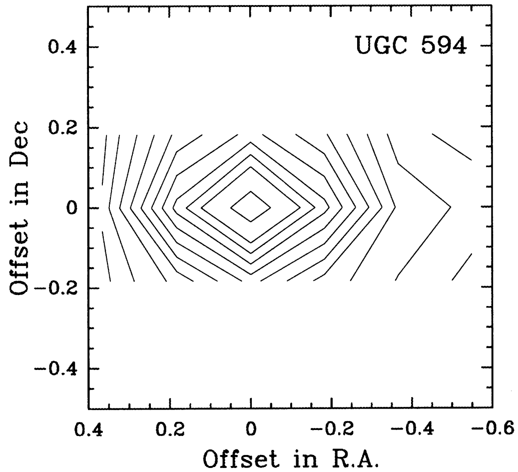

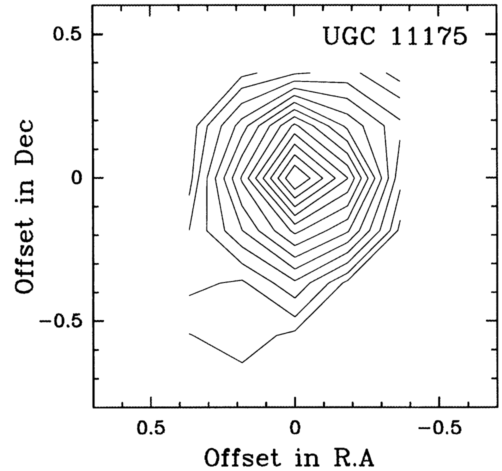

FIG. 4.—CO (1–0) contour map of UGC 594 (*left*) and UGC 11175 (*right*) observed with the IRAM 30 m telescope. The offsets are in arcminutes.

Most of the galaxies observed with the 30 m telescope are smaller than 1′ and were observed with a single pointing. Galaxies larger than 1′ were observed mostly with the 12 m telescope, but some were also mapped with the 30 m telescope. Close pairs, (e.g., UGC 8774), that could not be resolved by the 12 m telescope were observed with the 30 m telescope, which provided sufficiently high resolution to resolve them.

The final spectra from the 30 m telescope were reduced using the CLASS software and are given in Figure 2. All the spectra were boxcar smoothed to a resolution of 10.4 km s^{-1}. The antenna temperatures T_a^* have been converted to main-beam temperature T_{mb} using the formula

$$T_{mb} = (F_{eff}/B_{eff})T_a^* = (0.92/0.75)T_a^* ,$$

where F_{eff} and B_{eff} are the forward efficiency and main-beam efficiency, taken from the manual of the IRAM 30 m telescope.

The systems UGC 594, UGC 11175, and UGC 12914/15 are quite extended and so were mapped in more detail. The grid maps of UGC 594 and UGC 11175 are shown in Figure 3, and their contour maps are shown in Figure 4. The system UGC 12914/15, called the "taffy galaxies" by Condon et al. (1993), has an outstanding morphology and will be discussed in detail in a separate paper.

4. THE CO (1–0) DATA

In Table 2A (for the NRAO survey) and Table 2B (for the IRAM survey) we present the parameters of the CO (1–0) line, including the central velocity (heliocentric), FWHM line width, peak temperature T_{mb}, rms noise level in T_{mb}, integrated line intensity, and its uncertainties. Also shown is the correction factor C defined as the ratio between the total CO flux and the flux within the telescope beam. S_{CO} and σ are the derived total CO flux and the corresponding rms noise. The last column is the confidence level, which represents the uncertainty in the correction factor. The derivation of the correction factor and the definition of the confidence level are given in § 5.

For most galaxies, the central velocity, line width, and peak temperature were derived by fitting a Gaussian profile. For the irregular profiles, the FWHM width and peak temperature were estimated visually. The integrated line fluxes are represented by the sums over all channels. The uncertainties in the integrated line intensities were determined using the following formulae:

$$\Delta I = (\Delta I_n^2 + \Delta I_b^2 + \Delta I_w^2)^{1/2} , \tag{1}$$

where

$$\Delta I_n = T_{rms} W[\Delta v/W]^{1/2} , \tag{2}$$

$$\Delta I_b = T_{rms} W[\Delta v/(B - W)]^{1/2} , \tag{3}$$

$$\Delta I_w = \langle T_{mb} \rangle \Delta W . \tag{4}$$

The quantity ΔI_n is the rms noise in the spectrum, ΔI_b is the uncertainty due to errors in the determination of the baseline, ΔI_w is the uncertainty due to errors in the determination of the line width, W is the velocity range over which the spectrum is integrated, Δv is the smoothed channel width, T_{rms} is the rms noise per channel in the smoothed spectrum, B is the total velocity range of the spectrometer, $\langle T_{mb} \rangle$ is the average main-beam temperature of the source, and ΔW is the uncertainty in the spectral line width.

The rms noise ΔI_n is usually less than 10% and is primarily weather dependent. The baseline uncertainty ΔI_b is typically 5%–10% but may be up to 25% for weak and broad spectral lines. The quantity ΔI_w is usually less than 5% for most galaxies and near 10% for several weak sources.

We note that there are other types of uncertainties of a systematic nature that are not included in Table 2. The uncertainty in absolute calibration is reflected by the uncertainty in the ratio of the measured main-beam temperature T_{mb} to the true flux density from the source. This ratio is 30.4 ± 6.1 Jy K^{-1} for the 12 m telescope and 5.1 ± 0.7 Jy K^{-1} for the IRAM 30 m telescope. The uncertainty in this ratio was estimated from observations of standard calibrators such as Mars, IRC+10216, Orion A, and many quasars. Secondly, the error in pointing will lead to a systematically lower line intensity I_{CO}. This effect is generally less than 15% when the pointing error is smaller than 11″ for the 12 m telescope and smaller than 4″ for the 30 m telescope.

Although most of the galaxies are only slightly larger than the telescope beam, a correction factor is needed to include CO emission not covered by the telescope beam.

TABLE 2A

CO Line Parameters for Galaxies Observed with the 12 m Telescope

Name	Offsets (arcsec)	V (km s^{-1})	ΔV[a] (km s^{-1})	$T^{p}_{\rm mb}$ (mK)	$\pm\sigma_T$	$I_{\rm CO}$[b] (K km s^{-1})	$\pm\sigma_I$	C[c]	$S_{\rm CO}$[d] (Jy km s^{-1})	$\pm\sigma$	Confidence Level[e]
UGC 365		4520	281	14.8	2.8	5.36	0.49	1.47	240.3	21.9	2
UGC 593		5210	391	3.4	1.7	1.34	0.30	[f]	<11.9	...	3
UGC 594		5129	380	16.1	2.2	6.02	0.40	1.05[f]	192.2	13.7	1
UGC 717		...	...	...	1.6	<0.74	...	1.25	<28.1	...	2
UGC 813		5125	178	8.4	1.7	1.82	0.23	0.77[f]	42.7	8.0	3
UGC 816		5250	310	12.7	2.5	4.08	0.41	1.29[f]	161.0	16.6	3
UGC 979		4716	180	12.2	2.7	2.05	0.34	1.45	90.1	14.9	3
UGC 1063		5770	135	11.6	2.4	1.41	0.26	1.11	47.5	8.8	3
UGC 1430		...	...	...	1.9	<1.02	...	1.36	<42.5	...	2
UGC 1810		7480	310	7.3	1.7	1.39	0.24	1.53	64.4	11.2	4
UGC 3031		...	...	...	2.1	<0.75	...	1.22	<27.8	...	2
UGC 3032		...	...	...	1.9	<1.02	...	1.16	<36.1	...	2
UGC 4264		4089	93	14.1	2.4	1.42	0.19	1.54	66.4	8.9	4
UGC 4653		...	...	...	4.0	<1.31	...	1.37	<54.5	...	2
UGC 4718		...	...	...	2.6	<1.36	...	1.16	<48.2	...	3
UGC 4744		2380	287	5.1	1.6	1.59	0.33	1.13	54.8	11.4	2
UGC 4757		...	...	...	2.5	<0.69	...	1.33	<27.9	...	3
UGC 5265		...	...	...	2.7	<0.66	...	1.16	<23.3	...	2
UGC 5269		1882	108	5.7	2.2	0.57	0.17	1.71	29.6	8.8	4
UGC 5600		2772	190	6.6	3.4	1.14	0.34	1.25	43.1	12.8	2
UGC 5609		...	...	...	2.4	<0.85	...	1.20	<31. 1	...	2
UGC 5773		...	...	...	1.6	<0.91	...	1.05	<28.9	...	2
UGC 5931		1617	200	6.8	2.7	1.32	0.25	1.44	57.6	10.9	4
UGC 5935		1681	39	18.5	4.3	0.76	0.18	1.70	39.3	9.3	4
UGC 6134		7725	246	7.4	2.0	2.16	0.39	1.38	90.8	16.4	3
UGC 6643		7102	181	9.1	2.2	1.59	0.25	1.29	62.5	9.8	3
UGC 8529	(0, 0)	2931	265	34.4	5.3	8.70	0.67	1.34[g]	362.7	27.3	3
	(0, −30)	2931	200	12.8	6.6	3.6	0.88				
	(0, 30)	2920	210	18.8	7.0	4.0	0.95				
	(30, 30)	...	...	...	6.6	<0.88	...				
	(−23, 30)	2900	213	19.3	7.6	6.30	0.99				
	(−53, 0)	2900	240	21.4	3.9	3.01	0.51				
UGC 8677		7597	307	6.8	1.7	2.05	0.26	1.23	76.5	9.7	2
UGC 8774		9900	450	12.7	2.8	5.86	0.54	1.03	184.5	17.0	2
UGC 8898		3454	77	64.8	6.8	5.06	0.42	1.31	201.3	16.7	3
UGC 8900	(0, 0)	3457	380	31.8	3.2	5.45	0.55	3.3[g]	547.8	55.2	3
	(0, +60)	3362	230	17.0	4.2	3.6	0.50				
	(0, −60)	3712	235	7.4	3.3	1.65	0.41				
UGC 8931		3680	450	3.4	1.6	1.14	0.33	1.23	42.7	12.4	2
UGC 9102		7610	406	9.7	1.5	3.63	0.37	1.00[h]	110.5	11.3	1
UGC 9142		3125	141	8.0	3.0	1.15	0.49	1.16	40.5	17.3	2
UGC 9226		3886	201	43.8	4.4	9.28	0.53	1.73	490.0	28.0	4
UGC 9507		9700	281	4.5	1.5	1.18	0.30	1.23	44.1	9.2	4
UGC 9851		2580	379	11.2	2.2	3.77	0.33	1.29	148.3	13.0	2
UGC 9903		2002	201	55.7	8.2	9.28	0.90	1.29[f]	364.5	37.3	3
UGC 9904	(0, 0)	1889	142	33.1	3.9	4.43	0.38	0.54[f]	72.8	13.5	2
	(−20, −10)	1920	178	43.2	4.5	7.98	0.43				
UGC 10033		3315	112	23.4	2.9	2.27	0.23	1.29	89.3	9.0	3
UGC 10267		8836	110	41.2	5.4	4.66	0.47	1.26	179.0	18.1	2
UGC 10607		10420	138	5.7	2.4	0.50	0.17	1.16	17.7	6.0	2
UGC 10610		10099	212	7.0	2.6	1.38	0.33	1.41	58.8	14.1	3
UGC 10923 W......		7894	139	25.2	5.1	3.68	0.52	1.15[f]	128.9	20.1	2
UGC 10923 E		...	...	...	3.6	<1.02	0.66	[f]	<31.5	...	2
UGC 11137		2280	150	14.0	2.7	2.20	0.27	1.35	90.4	11.1	3
UGC 11175 S.......		6180	410	8.0	2.3	2.57	0.36	0.44[f]	34.4	14.3	2
UGC 11175 N		6120	330	19.9	3.4	6.53	0.52	1.09[f]	219.3	17.3	2
UGC 11391	(0, 0)	4552	305	11.4	2.6	2.05	0.38	1.46[g]	90.9	16.9	3
	(0, 30)	4558	120	3.4	1.5	0.63	0.21				
	(−30, −30)	4465	180	4.5	2.0	1.0	0.26				
UGC 11414		...	...	...	2.5	<0.86	...	1.18	<31.0	...	2
UGC 11657		...	...	...	1.6	<0.70	...	1.21	<25.9	...	2
UGC 11984		4546	420	19.1	2.5	4.80	0.40	1.23[f]	179.5	15.1	2
UGC 11985		4531	263	4.2	1.7	1.35	0.85	1.15[f]	47.3	31.5	2
UGC 12066		5634	118	7.7	1.7	1.06	0.19	1.15	36.9	6.6	2

TABLE 2A—*Continued*

Name	Offsets (arcsec)	V (km s^{-1})	ΔV[a] (km s^{-1})	T^{p}_{mb} (mK)	$\pm\sigma_T$	I_{CO}[b] (K km s^{-1})	$\pm\sigma_I$	C[c]	S_{CO}[d] (Jy km s^{-1})	$\pm\sigma$	Confidence Level[e]
UGC 12456		...	...	...	1.4	<0.80	...	1.28	<31.0	...	2
UGC 12457	(0, 0)	4710	260	16.4	2.8	4.43	0.38	1.59[f]	214.5	18.4	3
	(10, 48)	4613	315	7.2	3.2	1.47	0.50			2	
UGC 12908		...	...	...	1.7	<0.98	...	1.19	<35.5	...	2
UGC 12911		4755	208	5.7	1.3	1.33	0.20	1.14[f]	45.6	7.0	2
UGC 12914		4480	360	21.5	4.0	9.15	0.80	1.51	419.7	36.7	3
UGC 12915		4551	224	39.7	7.0	10.45	1.20	1.20	381.3	43.8	2

[a] FWHM.
[b] All the upper limits in I_{CO} are estimated as a 3 σ level using the H I line width in Table 1 (or assumed to be 500 km s^{-1} when the H I line width is not available).
[c] Correction factor. The derivation of this factor is given in § 5.
[d] Total CO flux after applying the correction factor. It is derived using the formula $S_{CO} = I_{CO}\,C30.4$ Jy K^{-1}.
[e] Represents the uncertainty in the derivation of the total CO flux by model fitting (see § 5.2).
[f] For close pairs of galaxies, the correction factor and total CO flux are derived from Table 3.
[g] The correction factor and total CO flux for galaxies with multiple sampling points were derived with a best-fit model. See Table 4 for details.
[h] UGC 9102 has been mapped by us with the OVRO interferometer, and the CO source size is less than 8″. Thus no correction is needed.

TABLE 2B

CO Line Parameters for Galaxies Observed with the IRAM 30 m Telescope

Name	V (km s^{-1})	ΔV[a] (km s^{-1})	T^{p}_{mb} (mK)	$\pm\sigma_T$	I_{CO}[b] (K km s^{-1})	$\pm\sigma_I$	C[c]	S_{CO}[d] (Jy km s^{-1})	$\pm\sigma$	Confidence Level[e]
UGC 593	...	...	...	2.8	<1.08	...	2.50	<13.9	...	3
UGC 594	Map[f]									
UGC 717	11645	363	6.7	2.6	2.45	0.33	2.22	28.0	4.6	4
UGC 816	5321	206	46.6	8.0	9.75	0.66	2.56	128.4	10.7	5
UGC 3706 N........	6263	331	7.9	3.0	2.09	0.38	1.11	11.9	2.7	2
UGC 3706 S	6185	121	15.9	2.9	1.75	0.16	1.11	10.0	1.1	2
UGC 5304 S	12261	213	6.6	2.6	1.54	0.25	1.82	1.43	2.6	4
UGC 5773	...	...	...	2.9	<1.04	...	1.27	<6.8	...	3
UGC 5984	10382	278	11.0	2.8	3.10	0.28	2.87	45.7	5.1	5
UGC 6527	...	...	...	8.0	<2.59	...	1.53	<20.4	...	3
UGC 7085A S	6954	283	24.2	3.5	6.96	0.39	3.30	117.9	8.1	5
UGC 7085A N......	...	...	...	1.8	<0.59	...	1.14	<3.5	...	2
UGC 7230 S	7128	35	17.7	2.9	0.55	0.08	2.14	6.1	1.1	5
UGC 7230 N........	...	...	...	3.3	<1.08	...	2.14	<11.9	...	5
UGC 7277 N........	...	...	...	2.3	<0.91	...	1.90	<8.9	...	4
UGC 7277 S	6691	228	14.2	3.0	3.26	0.26	2.79	46.7	4.6	5
UGC 8357 S	9955	337	41.1	5.5	13.91	0.66	1.70	121.5	7.1	4
UGC 8774 S	9945	431	55.9	5.1	24.62	0.86	1.06[g]	133.9	4.7	1
UGC 8774 N........	9890	410	25.5	4.0	11.86	0.76	1.08[g]	65.8	4.2	1
UGC 8849 S	...	...	...	3.4	<1.05	...	1.56	<8.4	...	3
UGC 8849 N........	...	...	...	2.6	<0.75	...	1.26	<4.8	...	2
UGC 8929 S	...	...	...	2.5	<0.87	...	1.27	<5.7	...	2
UGC 8941 N........	7970	253	39.5	3.3	8.81	0.49	2.06[h]	93.2	5.1	4
UGC 8941 S	7909	298	7.7	2.0	2.36	0.22	0.56[h]	6.7	1.7	4
UGC 9000	...	...	...	3.0	<0.97	...	1.43	<7.1	...	3
UGC 9001	11401	180	26.4	3.8	4.07	0.28	1.51	31.6	2.7	3
UGC 9102	7618	393	55.3	10.3	19.96	0.93	1.05[g]	107.8	5.0	1
UGC 9525	8392	375	11.4	3.3	5.50	0.54	2.06	58.1	7.0	5
UGC 10675	10120	214	16.7	2.2	3.74	0.18	1.33	25.5	1.5	3
UGC 11175	Map[f]									
UGC 11657	5818	93	8.7	2.5	0.81	0.12	2.06	8.6	1.6	5
UGC 11658	5794	79	25.4	2.7	2.29	0.15	2.14	25.2	2.0	5
UGC 11695	9576	311	30.7	3.0	9.81	0.36	2.06	103.9	4.7	5

[a] FWHM.
[b] All the upper limits in I_{CO} are estimated as a 3 σ level using the H I line width in Table 1 (or assumed to be 500 km s^{-1} when the H I line width is not available).
[c] Correction factor. The derivation of this factor is given in § 5.
[d] Total CO flux after applying the correction factor. It is derived using the formula $S_{CO} = I_{CO}\,C30.4$ Jy K^{-1}.
[e] Represents the uncertainty in the derivation of the total CO flux by model fitting (see § 5.2).
[f] The total CO fluxes are given in Table 4 for UGC 594 and UGC 11175.
[g] UGC 8774 and UGC 9102 have been mapped by us with the OVRO, and we use the sizes measured from the interferometer map to calculate the correction factors.
[h] For close pairs the correction factor and total CO flux are derived from Table 3.

We have estimated this correction factor for each galaxy in Tables 2A and 2B. The derivation of this factor is described next.

5. DERIVATION OF GLOBAL CO FLUXES

5.1. *The Correction Factor*

The correction factor is the ratio between the derived global CO flux and the measured flux within the telescope beam. We used a method similar to that of Young et al. (1995) to derive the total CO flux for each galaxy. We assume that the molecular gas is distributed in an azimuthally symmetric thin disk with either an exponential or a Gaussian radial distribution. The inclination angle, position angle, and size of the optical disk for each galaxy were taken from RC3 (or from the NASA/IPAC Extragalactic Database [NED][7] and the UGC catalog when the RC3 data were not available). The size of the CO disk is parameterized by a characteristic scale parameter D_0. For an exponential distribution, D_0 is twice the exponential scale length; for a Gaussian distribution, D_0 is the FWHM. We denote f as the ratio between the size of the optical disk D_{25} and D_0, i.e., $f = D_{25}/D_0$. We can distinguish three different cases.

(1) For galaxies with a single pointing measurement, we use the exponential model with $f = 5$ to estimate the correction factor for each galaxy. Such a model is adopted because Young et. al. (1995) found that more than 50% of the galaxies with multiple sampling points in the FCRAO survey were best fitted by an exponential model, with an average value $f = 5$. We have tried both the Gaussian and exponential models with different f factors for every galaxy and found that the correction factor varies by less than 40% in most cases. A detailed discussion of the uncertainty in the derived total flux is in § 5.2.

(2) For paired galaxies with a separation comparable with the size of the telescope beam, the CO emission from both components will contribute to the measured flux even though the telescope beam was centered on one of the galaxies. For these sources, we made two measurements with the pointing centers on the nucleus of each galaxy, then estimated the total CO flux for each individual galaxy using the method described in the Appendix. Table 3 lists the input parameters used and the integrated line intensities derived with an exponential model with $f = 5$, except for UGC 593/4 and UGC 11175, for which a Gaussian model was used, as explained below.

(3) For each galaxy observed at multiple positions, we obtain a better constraint on the parameter f and the central peak position (x_0, y_0) of the CO brightness distribution. The galaxies UGC 594, UGC 8529, and UGC 11175 were observed at more than five points, and thus we can estimate f, (x_0, y_0), and the inclination angle i using the method of least-squares fitting. The sources UGC 8900 and UGC 11391 have measurements at three points, and thus we can estimate f and y_0. UGC 12457 was measured at only two points, and only the value of y_0 can be constrained. In addition, UGC 594 and UGC 11175 were fully sampled with the IRAM telescope, so we can directly obtain the total CO flux by summing over the CO flux measurements in each half-beam cell (Tables 2C and 2D). The total flux obtained directly from the map is consistent with the flux derived through model fitting in Table 4.

For each galaxy, we tried fitting the data with both Gaussian and exponential models. Table 4 lists the best-fit model with the corresponding parameters and the derived total CO fluxes for each galaxy. All galaxies can be fitted reasonably well with either a single-component Gaussian or exponential model. For the three galaxies with more than five pointings, we found that the position angle of the CO disk is similar to that of the optical disk, but two galaxies (UGC 8925 and UGC 11175) were found to have a different inclination angle for the CO disk than that of the optical disk. It is interesting to note that all three galaxies are best fitted with a Gaussian model.

5.2. *Uncertainties in the Global CO Fluxes*

The uncertainty in the correction factor arises mainly from the uncertainty in the choice of models and the input parameters. Many IGs have strongly disturbed morphology, and the size of the optical disk is not very well determined. This will give an even larger uncertainty in the CO

[7] NED is operated by the Jet Propulsion Laboratory, California Institute of Technology, under contract with the National Aeronautics and Space Administration.

TABLE 2C

CO LINE PARAMETERS FOR UGC 594 MAPPED WITH THE IRAM 30 m TELESCOPE

Offsets (arcsec)	V (km s^{-1})	ΔV (km s^{-1})	$T^p_{\rm mb}$ (mK)	$\pm\sigma T$	$I_{\rm CO}$ (K km s^{-1})	$\pm\sigma I$
0, 0	5088	368	81.7	8.3	31.53	1.05
0, 11	5121	355	48.9	6.7	16.83	0.77
0, −11	5079	310	48.0	6.9	14.41	0.77
11, 0	5046	333	59.9	9.0	19.31	1.15
11, 11	5063	348	34.7	6.0	11.72	0.97
11, −11	5013	240	29.8	6.0	6.92	0.98
22, 0	4994	148	14.8	6.2	2.12	1.21
−11, 0	5166	306	59.3	8.5	19.30	1.06
−11, 11	5197	306	38.3	4.9	11.38	0.70
−11, −11	5196	284	27.5	6.0	7.56	1.03
−22, 0	5253	106	54.4	5.9	5.60	0.60
−22, 11	5257	101	24.1	5.7	2.37	0.97
−22, −11	5246	91	39.6	4.8	3.52	0.55
−33, 0	5253	136	22.1	6.2	2.91	0.98
Total	CO flux $S_{\rm CO} = 198 \pm 16$ Jy km s^{-1}					

TABLE 2D

CO LINE PARAMETERS OF UGC 11175 MAPPED WITH THE IRAM 30 m TELESCOPE

Offsets (arcsec)	V (km s^{-1})	ΔV (km s^{-1})	$T^{p}_{\rm mb}$ (mK)	$\pm\sigma_T$	$I_{\rm CO}$ (K km s^{-1})	$\pm\sigma_I$
0, 0	6169	346	103.0	8.8	33.70	1.19
0, 11	6106	302	68.7	8.0	21.48	1.20
0, 22	6087	259	14.2	7.3	3.29	1.18
0, −11	6194	343	59.2	8.4	19.09	1.14
0, −22	6214	454	17.6	9.3	5.01	2.70
11, 0	6201	337	50.4	7.8	16.30	1.18
11, 11	6174	298	33.6	7.9	9.70	1.12
11, −11	6276	216	50.7	7.5	10.95	1.16
11, −22	6307	85	35.2	7.2	3.25	1.11
11, −33	6257	333	11.5	6.1	2.98	0.92
11, −43	...	...	...	5.5	<2.2	0.82
22, 0	...	...	...	8.6	<2.5	1.17
22, 11	...	...	...	6.4	<2.3	1.09
22, −11	6322	101	31.8	6.6	3.72	1.14
22, −22	6211	297	15.2	6.4	4.28	0.93
22, −33	...	...	...	6.4	<2.3	0.89
−11, 0	6124	312	80.2	8.9	23.40	1.17
−11, 11	6046	226	55.5	8.3	12.84	1.16
−11, 22	6040	222	22.1	7.5	4.59	1.17
−11, −11	6169	326	41.6	7.8	13.90	1.20
−22, 0	6035	178	24.8	8.5	4.38	1.16
−22, 11	6014	365	18.0	8.0	4.06	1.50
−22, 22	...	...	...	6.1	<2.2	0.92
Total	CO flux $S_{\rm CO} = 254 \pm 29$ Jy km s^{-1}					

source size and morphology. However, aperture synthesis studies show that the CO distribution in IGs is usually more compact than in normal spiral galaxies (see the review by Young & Scoville 1991). A compact source is usually better modeled by the Gaussian distribution, as in the case of the three IGs we measured with more than five sampling points (Table 4). Our calculation shows that the correction factors estimated using a Gaussian model with $f = 3, 4, 5, 6$ are smaller than that given by our default exponential model with $f = 5$. Therefore, using the correction factor listed in Tables 2A and 2B may overestimate the total CO fluxes if the CO brightness distribution is more compact or closer to the Gaussian model, but the differences are usually less than 30%. On the other hand, if the CO distribution is

TABLE 3

MODELING PARAMETERS AND CORRECTION FACTORS FOR CLOSE GALAXY PAIRS

Name (1)	Model (2)	f (3)	P.A. (4)	r_1 (5)	r_2 (6)	I (7)	I_0 (8)	C (9)	Confidence Level (10)
UGC 593	G	4.0	0	1.4	1.3	1.34	<0.39	...	3
UGC 594	G	4.0	105	1.1	0.7	6.02	6.32	1.05	1
UGC 813	E	5.0	115	1.2	0.5	1.82	1.40	0.77	2
UGC 816	E	5.0	0	1.9	1.0	4.08	5.26	1.29	2
UGC 8941 N	E	5.0	140	1.1	1.1	8.81	18.13	2.06	3
UGC 8941 S	E	5.0	20	0.2	0.2	2.36	1.32	0.56	3
UGC 9903	E	5.0	169	1.6	1.4	9.28	11.97	1.29	2
UGC 9904	E	5.0	1.3	0.6	3.9	4.43	2.39	0.54	2
UGC 10923 W......	E	5.0	4	1.2	0.7	3.68	4.23	1.15	2
UGC 10923 E	E	5.0	0	0.5	0.3	<1.02	<1.02	...	2
UGC 11175 N	G	8.5	189	2.0	0.8	6.53	7.21	1.09	2
UGC 11175 S	G	8.5	0	0.5	0.4	2.57	1.00	0.44	2
UGC 11984	E	5.0	118	1.7	0.5	4.80	5.90	1.23	2
UGC 11985	E	5.0	55	1.6	0.5	1.35	1.55	1.15	2
UGC 12911	E	5.0	10	1.1	0.8	1.33	1.52	1.14	2
UGC 12908	E	5.0	0	1.2	0.9	<0.98	<0.98	...	2

NOTE.—Col. (1): Galaxy identification by UGC number. Col. (2): Model for the molecular gas distribution. G represents a Gaussian model, and E represents an exponential model. For UGC 594 and UGC 11175, the parameters were taken from Table 4. Col. (3): Defined in § 5.1 Col. (4): Position angle, in degrees. Col. (5): Size of the optical disk on the major axis, in arcminutes. Col. (6): Size of the optical disk on the minor axis, in arcminutes. Col. (7): Observed integrated line intensities in, K km s^{-1}, on the scale of main-beam temperature $T_{\rm mb}$. Col. (8): Intrinsic line intensities, in K km s^{-1}, on the scale of main-beam temperature $T_{\rm mb}$. Col. (9): Correction factor. For the nondetection cases, no corrections were applied to the upper limits.

TABLE 4

BEST-FIT MODEL AND PARAMETERS FOR GALAXIES WITH MULTIPLE SAMPLING POINTS

Name (1)	Model (2)	f (3)	P.A. (4)	D_{25} (5)	i (6)	x_0 (7)	y_0 (8)	S_{CO} (9)	Confidence Level (10)	χ^2_ν (11)
UGC 594	G	4.0	105	1.1	24	−0.5	1.2	208	1	2.3
UGC 8529	G	5.5	100	1.8	90	−14	3.1	354	2	1.9
UGC 8900	E	2.6	167	2.9	31	...	17	548	3	...
UGC 11391......	E	3.2	30	1.0	24	...	−16	91	2	...
UGC 11175......	G	8.5	190	2.0	49	−2.1	−0.5	246	1	1.5
UGC 12457......	E	4.6	10	2.8	15	...	0.	215	3	...

NOTE.—Col. (1): Galaxy identification by UGC number. Col. (2): Model for the molecular gas distribution. G represents a Gaussian model, and E represents an exponential model. Col. (3): Defined in § 5.1 Col. (4): Position angle, in degrees. Col. (5): Size of the optical disk on the major axis, in arcminutes. Col. (6): Inclination angle, in degrees. Cols. (7), (8) Offset (x_0, y_0) of the CO peak from the center of the telescope beam, in arcseconds. Col. (9): Total CO flux derived with the best-fit model.

more extended than in our model, we would underestimate the total CO flux. An extreme case is UGC 8900, which is best fitted by an exponential model with $f = 2.6$. Using the average value $f = 5$ would underestimate the total CO flux by a factor of 2 in this galaxy.

For the galaxies with multiple sample points, the input parameters are constrained more tightly, and therefore the uncertainty in the total CO flux is smaller. In the best cases (UGC 594 and UGC 11175), the brightness distributions are fully sampled with the 30 m telescope, and more than 90% of the flux has been sampled. Thus the correction is small, and the uncertainty in the total CO flux is less than 10%. For the other four galaxies except UGC 12547, the factor f can be constrained within ± 1, so the uncertainty in the correction factor due to the uncertainty in the factor f is less than 20%.

For the close pairs, the uncertainty in the correction factor is similar to that of a galaxy with two point measurements. This is usually around 20%, except for UGC 594 and UGC 11175, where it is less than 10%, as discussed above.

There are other sources of uncertainty. If the peak of the CO brightness distribution is not at the nucleus, our regular observations with the telescope beam pointing to the galaxy center may have missed a significant amount of the CO flux. This situation is similar to that when the telescope is not pointing properly to the source because of pointing errors. Young et al. (1995) found that fewer than 20% of the galaxies they mapped exhibit a CO brightness peak outside the nuclear region, and only one galaxy has its CO peak more than 10 kpc away from the galaxy nucleus. But in interacting systems, an off-center CO peak is more common. For the five galaxies we observed with at least three points, three galaxies (UGC 8529, UGC 11391, and UGC 8900) were found to have their CO peak offset from the nucleus by 14″–17″ (see Table 4). If we use the correction factor derived by assuming that the telescope was centered at the CO peak, we would underestimate the total CO flux by 9%–17% in these galaxies. In general, the uncertainty due to the offset between the CO peak and the telescope beam should be less than 30%.

Finally, the brightness distribution may not be azimuthally symmetric, and it may correspond to neither a Gaussian nor an exponential form. However, as noted earlier, the molecular gas distribution tends to be more compact in IGs, so the correction factor would be more close to unity regardless which model is appropriate. The correction factors used in Tables 2A and 2B are often not much higher than unity. Hence the overestimates, if any, in the correction factor would not be serious for most cases. In addition, any overestimates in the total CO flux may be partly offset by the underestimates because of pointing errors or noncentral distributions.

In order to more quantitatively estimate the uncertainty in the derived global CO flux, we have performed a Monte Carlo test of the variation of the correction factor. For each galaxy, we change the input parameters f, (x_0, y_0), and i randomly with both Gaussian and exponential models. The modeling uncertainties were classified into five categories, each associated with a "confidence level." If the variation of the correction factor is less than 10%, the confidence level is assigned as 1. If the variation is in the range of 10%–20%, 20%–30%, or 30%–40%, the confidence level is 2, 3, or 4, respectively. A confidence level of 5 is the highest level and indicates that the modeling uncertainty is 40%–60%. Only galaxies with detailed mapping data have a confidence level of 1, and most galaxies have a confidence level of 2–4 (Tables 2A and 2B). A large uncertainty in the correction factor arises when the source size is much larger than the telescope beam. This is the case for several galaxies observed with the IRAM 30 m telescope, and therefore their confidence levels are 5 (Table 2B). All galaxies observed with the 12 m telescope have a confidence level less than 5.

The total uncertainty in the derived global CO flux would be the quadratic sum of the rms noise, the uncertainty in absolute calibration, and the uncertainty in the modeling. For most galaxies the total uncertainties are less than 40% but could be as high as 60% for extreme cases.

6. GALAXIES OBSERVED WITH BOTH THE 12 AND 30 m TELESCOPES

Several galaxies were observed with a single pointing using the NRAO 12 m telescope and also mapped at high resolution with the IRAM 30 m telescope (Table 5). Comparing the data taken with different telescopes provides a good test for the methods used to derive the total CO fluxes, and it also gives some indication regarding the reliability of the uncertainty estimates.

The close pairs UGC 593/4 and UGC 11175 were observed with double pointings by the NRAO 12 m and fully sampled by the IRAM 30 m telescope. The beam of the 30 m telescope is small enough to resolve these pairs, and the contamination from the nearby component is negligible. UGC 593 and UGC 11175S were not detected with the 30 m telescope ($3\sigma < 13.9$ Jy km s^{-1} for UGC 593 and <25.2 Jy km s^{-1} for UGC 11175). Their CO fluxes derived from the 12 m data after correcting the contamination from UGC

TABLE 5

COMPARISON OF THE TOTAL CO FLUX FOR GALAXIES OBSERVED WITH BOTH THE 12 AND 30 m TELESCOPES

Name	NRAO 12 m S_{CO} (Jy km s^{-1})	IRAM 30 m S_{CO} (Jy km s^{-1})
UGC 593	<11.9	<13.9
UGC 594	192.2 ± 40.9	208.1 ± 33.1
UGC 717	<28.1	28.0 ± 5.8
UGC 816	128.4 ± 27.7	161.0 ± 28.0
UGC 5773	<29.1	<6.8
UGC 8774	184.5 ± 40.6	199.7 ± 29.3
UGC 9102	110.5 ± 24.8	107.8 ± 15.9
UGC 11175 N	219.3 ± 47.5	254.6 ± 45.9
UGC 11175 S	34.6 ± 16.8	<25.2
UGC 12914/15......	801.0 ± 180.1	1012.1 ± 171.6

NOTE.—The calibration uncertainties have been included in the values listed here.

594 and UGC 11175 N were less than 11.9 Jy km s^{-1} for UGC 593 and 34.6 ± 17 Jy km s^{-1} for UGC 11175 (Table 3), which are consistent with the 30 m measurements given the combined uncertainties. The marginal discrepancy between the two measurements for UGC 11175 S indicates that our model may underestimate the contamination from UGC 11175 N.

The total CO flux derived from the 12 m data (including calibration uncertainties) is 192 ± 41 Jy km s^{-1} for UGC 594 and 219 ± 47 Jy km s^{-1} for UGC 11175 (Table 2A). The IRAM 30 m maps yield $S_{CO} = 198 \pm 32$ Jy km s^{-1} for UGC 594 (Table 2C) and 254 ± 46 Jy km s^{-1} for UGC 11175 (Table 2D), which is consistent with the NRAO 12 m data. Again, we find that the 12 m telescope measurements and analysis underestimate the total CO flux in UGC 11175 N by 15%. This can partly be accounted for by the fact that the 12 m telescope was positioned ($-5''$, $+3''$) away from the CO peak of the IRAM 30 m map. Although the 30 m data indicate that UGC 11175 N would be fitted better by a Gaussian distribution with $f \simeq 8.5$ and an inclination angle $i = 49°$, we nevertheless find that the exponential model with $f = 5$ and $i = 23°$ (the inclination angle of the optical disk) would yield a global CO flux of 252 Jy km s^{-1} for UGC 11175 N using the 12 m data, which is surprisingly consistent with that from the IRAM 30 m data. This suggests that the errors in the correction factors listed in Tables 2A and 2B are not larger than our estimates of the uncertainties.

The total CO fluxes derived from different telescopes are also consistent for UGC 717, UGC 5773, UGC 8774, UGC 9102, and UGC 12914/15 (Table 5). We have fully mapped UGC 12914/15 (the "taffy galaxies") with the IRAM 30 m telescope, and the CO distribution in this system was found to be very asymmetric, with large amounts of molecular gas located in the region between the two optical disks of UGC 12914 and UGC 12915. Even in this extreme case, the derived global CO fluxes from the 12 m data using the correction factor from Table 2A are only 20% lower than the direct measurements from the IRAM 30 m map. This difference is consistent with our estimated uncertainties. Only the measurements for UGC 816 show a relatively larger discrepancy (25%), which is mainly due to the large uncertainty (confidence level, 5) in the IRAM 30 m measurements, as the source size is much larger than the telescope beam.

We conclude that the total CO fluxes derived from different telescopes are consistent with each other. Hence we have combined these two data sets into a large sample for a statistical study.

7. COMPARISONS WITH OTHER OBSERVATIONS

There are many CO surveys of galaxies reported in the literature. Most of them are focused on isolated galaxies, but some interacting systems have also been observed. The FCRAO Extragalactic CO Survey (Young et al. 1995) included 15 IGs. Braine & Combes (1993) observed 14 IGs in the IRAM 30 m CO survey, and Solomon & Sage (1988) observed 22 *IRAS*-selected IGs using the NRAO 12 m or the FCRAO 14 m telescope. Bushouse et al. (1999) also observed 25 galaxies in their sample in 1988 using the NRAO 12 m. We did not observe most of the IGs with good CO (1–0) published spectra, but we reobserved some galaxies in order to compare our data with that of other investigators. In addition, we reobserved the archetypical *IRAS*-luminous mergers Arp 220 and NGC 1614, which have been observed repeatedly by many groups with different telescopes.

Table 6 shows a comparison between the observed CO fluxes (without correction) measured by us and those reported by other investigators with the NRAO 12 m telescope or FCRAO 14 m telescope. Six galaxies were observed by both Bushouse et al. in 1988 and ourselves (both cases with the NRAO 12 m telescope). Three (UGC 10923, UGC 11175, and UGC 816) agree within 10% in the

TABLE 6

COMPARISON OF OUR MEASURED CO FLUXES WITH DATA IN THE LITERATURE

Name	This Work, 12 m	B99, 12 m	Y95, 14 m	S91, 12 m	SS88, 12 m
NGC 1614	206	262	241	301	101
UGC 816	124	112	…	…	…
UGC 9903	282	…	227	…	109
UGC 9904	135	…	…	…	97
UGC 10269......	142	…	145	151	…
UGC 10923......	112	113	…	…	…
UGC 11175......	199	172	…	144	…
UGC 12914......	278	210	…	…	…
UGC 12915......	318	507	…	…	…
Arp 220	412	…	403	301	…

NOTE.—The values are the measured CO fluxes in Jy km s^{-1} (without correction).

REFERENCES.—B99: Bushouse et al. 1999; Y95: Young et al. 1995; S91: Sanders et al. 1991; SS88: Solomon & Sage 1988.

integrated line intensity, and the other three (UGC 12914, UGC 12915, and NGC 1614) are within 20%–25%. As mentioned above, the CO distribution in UGC 12914/15 is very extended and asymmetric, so the two different observations with pointing errors emphasizing two different regions could easily give line intensities that differ by more than 20%.

Our measurements are also consistent (within 25%) with the data of Young et al. (1995) using the 14 m telescope and that of Sanders et al. (1991) using the 12 m telescope. Only the results reported by Solomon & Sage (1988) show a large discrepancy with our data as well as with other investigators' measurements. In particular, we found a large deviation in the measured CO fluxes for NGC 1614.

We conclude that the CO fluxes measured by us are consistent with most of the data in the literature within the quoted uncertainties. We will use the isolated spiral galaxies observed by Young et al. (1995) as a control sample to compare with the IGs sample that contains the IGs observed by us as well as by other investigators. The result of the statistical analysis will be reported in Paper II.

We thank the staff of the NRAO 12 m and IRAM 30 m telescopes for their assistance in obtaining these observations. In particular we thank Jeff Mangum for his help in estimating the calibration uncertainties of the NRAO 12 m telescope. This work was supported by a grant to E. R. S. from the Natural Sciences and Engineering Research Council of Canada. This research has made use of the NED, which is operated by the Jet Propulsion Laboratory, California Institute of Technology, under contract with the National Aeronautics and Space Administration.

APPENDIX

METHOD OF DERIVING THE CO FLUX FOR INDIVIDUAL GALAXIES IN CLOSE PAIRS

We denote (x_1, y_1) and (x_2, y_2) as the central positions of two galaxies G_1 and G_2 in a pair. We have made two measurements for each pair with the telescope pointing to (x_1, y_1) and (x_2, y_2). The measured integrated line intensities are denoted as I_1 and I_2, respectively. Each of these observed line intensities has contributions from both galaxies, and they are related to the intrinsic integrated line intensities I_{01} and I_{02} as follows:

$$\left\{\begin{array}{l} I_1 = a_{11} I_{01} + a_{12} I_{02} \\ \\ I_2 = a_{21} I_{01} + a_{22} I_{02} \end{array}\right\}, \tag{A1}$$

where a_{ij} is the contribution of the CO flux from galaxy G_j at (x_j, y_j) to the measurement centering at (x_i, y_i), where (and hereafter) $i, j = 1, 2$.

Let $T_i(x, y)$ be the brightness temperature distribution of galaxy G_i and $B_i(x, y)$ is its normalized form, i.e., $T_i(x, y) = T_i(0, 0)B_i(x, y)$. The intrinsic integrated line intensities I_{0i} for galaxy G_i are

$$I_{0i} = W_i \frac{2k}{\lambda^2} T_i(0, 0) \iint B_i(x, y) dx\, dy , \tag{A2}$$

where W_i is the spectral line width (FWZM) of galaxy G_i.

The coefficiencies a_{ij} can be specified as

$$a_{ij} = \frac{\iint_{-\infty}^{+\infty} P(x - x_i, y - y_i) B_j(x - x_j, y - y_j) dx\, dy}{\iint_{-\infty}^{+\infty} B_j(x, y) dx\, dy} , \tag{A3}$$

where $P(x, y)$ is the normalized beam pattern and is assumed to be Gaussian. Obviously, the coefficients a_{ij} depend only on the geometrical distribution of the brightness temperature and the antenna beam, not on the absolute intensity of each galaxy.

For a Gaussian distribution,

$$B(x, y) = \exp\left[(-4 \ln 2)\left(\frac{x^2}{D_0^2} + \frac{y^2}{D_0^2 \cos^2 \alpha}\right)\right], \tag{A4}$$

where D_0 is the FWHM of the Gaussian source and α is the inclination angle. In this case, the coefficients can be evaluated analytically, yielding

$$a_{ij} = \left(\frac{1}{[1 + (D_0/\theta_{\rm mb})^2]\{1 + [(D_0 \cos \alpha)/\theta_{\rm mb}]^2\}}\right)_j^{1/2} \exp\left[(-4 \ln 2)\left(\frac{\Delta x^2}{D_0^2 + \theta_{\rm mb}^2} + \frac{\Delta y^2}{D_0^2 \cos^2 \alpha + \theta_{\rm mb}^2}\right)\right]_j , \tag{A5}$$

where

$$\left\{\begin{array}{l} \Delta x = (x_i - x_j) \sin ({\rm PA}) - (y_i - y_j) \cos ({\rm PA}) \\ \Delta y = (x_i - x_j) \cos ({\rm PA}) + (y_i - y_j) \sin ({\rm PA}) \end{array}\right\} . \tag{A6}$$

The quantity $\theta_{\rm mb}$ is the main-beam diameter (FWHM), and PA is the position angle. The subscript j indicates that the value of D_0, α, and PA is for galaxy G_j.

In the case of the exponential model, the integration in equation (A3) was carried out numerically.

From equation (A2) we have

$$\left\{\begin{aligned} I_{01} &= \frac{a_{22} I_1 - a_{12} I_2}{a_{11} a_{22} - a_{21} a_{12}} \\ I_{02} &= \frac{a_{21} I_1 - a_{11} I_2}{a_{21} a_{12} - a_{11} a_{22}} \end{aligned}\right\} . \tag{A7}$$

REFERENCES

Barnes, J., & Hernquist, L. 1991, ApJ, 370, L65
———. 1992, ARA&A, 30, 705
Braine, J., & Combes, F. 1993, A&A, 269, 7
Bushouse, H. A. 1986, AJ, 91, 255
———. 1987, ApJ, 320, 49
Bushouse, H. A., Lord, S. D., Lamb, S. A., Werner, M. W., & Lo, K. Y. 1999, in preparation
Combes, F., Prugniel, P., Rampazzo, R., & Sulentic, J. W. 1994, A&A, 281, 725
Condon, J. J., Helou, G., Sanders, D. B., & Soifer, B. T. 1993, AJ, 105, 1730
de Vaucouleurs, G., de Vaucouleurs, A., Corwin, J. R., Buta, R. J., Paturel, G., & Fouqué, P. 1991, Third Reference Catalogue of Bright Galaxies (New York: Springer) (RC3)
Mihos, J. C., & Hernquist, L. 1994, ApJ, 431, L9
Nilson, P. 1973, Uppsala General Catalogue of Galaxies (Uppsala: Uppsala Obs.)
Sanders, D. B., Scoville, N. Z., & Soifer, B. T. 1991, ApJ, 370, 158
Sanders, D. B., Soifer, B. T., Elias, J. H. Madore, B. F., Matthews, K., Neugebauer, G., & Scoville, N. Z. 1988, ApJ, 325, 74
Solomon, P. M., & Sage, L. J. 1988, ApJ, 334, 613
Toomre, A., & Toomre, J. 1972, ApJ, 178, 623
Tremaine, S. 1981, in Proc. Advanced Study Institute, The Structure and Evolution of Normal Galaxies; ed. S. M. Fall & D. Lynden-Bell (Cambridge: Cambridge Univ. Press), 67
Young, J. S., Allen, L., Kenney, J. D. P., Lesser, A., & Rownd, B. 1996, AJ, 112, 1903
Young, J. S., et al. 1995, ApJS, 98, 219
Young, J. S., & Scoville, N. Z. 1991, ARA&A, 29, 581